Title page

Physiologically-Based Pharmacokinetics of Dexamethasone in Rats

Dawei Song[1#], Le Sun[1#], Debra C DuBois [1,3], Richard R Almon [1,3], Shengnan Meng [2], William J Jusko [1]

[1] Department of Pharmaceutical Sciences, School of Pharmacy and Pharmaceutical Sciences, State University of New York at Buffalo, Buffalo, NY, 14214, USA

[2] Department of Pharmaceutics, School of Pharmacy, China Medical University, Shenyang 110122, China

[3] Department of Biological Sciences, State University of New York at Buffalo, Buffalo, NY, 14260, USA

[#] Authors have contributed equally to these studies

1

Running title page

a) **Running title:** PBPK model of dexamethasone in rats

b) **Corresponding Author:**

William J Jusko, Ph.D., Department of Pharmaceutical Sciences, School of Pharmacy and

Pharmaceutical Sciences, State University of New York at Buffalo

Mailing Address: 404 Pharmacy Building, Buffalo, NY 14214-8033

Telephone: 716-645-2855, Fax: 716-829-6569, E-mail: wjjusko@buffalo.edu

c) **The number of text page:** 26

The number of tables: 2

The number of figures: 4

The number of references: 37

The number of words in the Abstract: 184

The number of words in the Introduction: 557

The number of words in the Discussion: 950

d) **Abbreviations used are:**

AUC: area under concentration curve

B/P: blood to plasma ratio

CYP: cytochrome P450

DEX: dexamethasone

PBPK: physiologically-based pharmacokinetics

P-gp: p-glycoprotein

PK: pharmacokinetics

SC: subcutaneous

Abstract

Blood and multi-tissue concentration-time profiles for dexamethasone (DEX), a synthetic corticosteroid, were measured in male rats after SC bolus and infusion dosing. A physiologically based pharmacokinetic (PBPK) model was applied for 12 measured tissues. Tissue partition coefficients (Kp) and metabolic clearance ($CL_{u,int}$) were assessed from infusion studies. Blood cell to plasma partitioning (0.664) and plasma free fraction (0.175) for DEX were found to be moderate. DEX was extensively partitioned into liver (Kp = 6.20), while the calculated Kp values of most tissues ranged between 0.1 and 1.5. Despite the moderate lipophilicity of DEX (Log P = 1.8), adipose exhibited very limited distribution (Kp = 0.17). Presumably due to p-glycoprotein mediated efflux, DEX concentrations were very low in brain compared to its expected high permeability. Infusion studies yielded Kp values from male and female rats at steady-state that were similar. In silico Kp values calculated for different tissues by using GastroPlus software were similar to in vivo values except for adipose and liver. Glucocorticoid receptors are found in diverse tissues and these PBPK modeling results may help provide exposure profiles driving pharmacodynamic effects of DEX.

Significance statement

Our PBPK model describes the experimentally determined tissue and plasma DEX PK profiles in rats reasonably well. This model can serve for further investigation of DEX tissue distribution in rats as the PK driving force for PD effects in different tissues. No major sex differences were found for DEX tissue distribution. Knowledge gained in this study may be translatable to higher-order species including humans.

Introduction

Corticosteroids (CS), first synthesized in the 1950s, are synthetic analogous of the endogenous glucocorticoid (GC) cortisol. In addition to rapid non-genomic effects, GC (and CS) bind to the ubiquitously expressed glucocorticoid receptors (GR) in the cytoplasm of various tissues (Oakley and Cidlowski, 2011). The GC-GR complexes then translocate into the nucleus, influencing downstream gene expression resulting in numerous biological effects in multiple tissues (Cato et al., 2002; Losel and Wehling, 2003; Baschant et al., 2012). The CS have strong immunosuppressive and anti-inflammatory properties, which provide the foundation for their wide application in conditions including organ transplants, rheumatoid arthritis, some lymphomas and many others (Rhen and Cidlowski, 2005; Kadmiel and Cidlowski, 2013). Further, CS are also used in non-immune related conditions, such as hormone replacement therapy for Addison's disease (Napier and Pearce, 2014) and promoting lung maturation to prevent respiratory distress syndrome in preterm births (Kadmiel and Cidlowski, 2013). However, high doses or chronic use of CS can magnify normal GC functions and elicit unwanted adverse effects such as osteoporosis, insulin resistance and growth retardation. Although their therapeutic effects are attractive and profound, the usefulness of CS is limited by dose and duration of regimens, calling for careful medical monitoring.

Since the success of early PBPK models in 1970s (Bischoff et al., 1970; Bischoff et al., 1971), pharmacokinetic (PK) profiles of many drugs have been successfully modeled by applying PBPK models (Sager et al., 2015). The most important properties of PBPK enable systems models based on physiological organ sizes and blood flow rates and provide insight regarding drug transport and permeability in various tissues, cells, and subcellular compartments depending on the measurements and model structures (Jones and Rowland-Yeo, 2013; Zhuang and Lu, 2016).

In addition, by adjusting parameters relevant to physiology, enzyme or transporter activity as well as physicochemical properties of the compounds, PBPK-based simulations can optimize properties of lead compounds, evaluate drug-drug interactions, and anticipate PK changes in special populations such as renal impairment (Jones et al., 2015; Zhuang and Lu, 2016).

As a potent synthetic CS, DEX is widely prescribed for different medical conditions and used in animal models. Previously, DEX plasma PK in healthy and arthritic rats as well as pregnant rats were explored thoroughly in our lab and corresponding drug effects at sites of action were assessed (Samtani and Jusko, 2005; Samtani et al., 2006; Earp et al., 2008; Song et al., 2018). However, tissue distribution of DEX has not been characterized in rats or other species to date. As the driving force for the downstream pharmacological effects, tissue PK profiles are the key to the establishment of mechanism-based relationships between pharmacological and toxicological effects and drug concentrations at the site of action.

Previous studies showed higher clearances in male rats compared to females based on plasma profiles for both DEX and methylprednisolone (Song et al., 2018; Ayyar et al., 2019a). Whether there exist sex differences in DEX tissue distribution has not been studied. Therefore, the purposes of the current study were: 1. Thorough investigation and description of multi-organ PK profiles of DEX in rats to seek a better understanding of determinants for DEX whole-body PK. 2. Comparison of tissue partition coefficients between females and males to augment previous PK studies of DEX in relation to sex in rats. 3. Obtaining a data base for possible scaling the PBPK of DEX to other species.

Methods

Chemicals and Reagents.

Pharmaceutical-grade dexamethasone sodium phosphate solution was purchased from Bimeda Pharmaceuticals (Dublin, Ireland). Dexamethasone-D5 (internal standard [IS], purity >98%) was obtained from Toronto Research Chemicals (Toronto, ON, Canada). Dexamethasone (purity > 98%) was purchased from Sigma-Aldrich (St Louis, MO). HPLC-grade methanol, acetonitrile and phosphoric acid were obtained from Fisher Scientific (Pittsburgh, PA). Milli-Q® water was used in the study (Millipore Corporation, Bedford, MA). Subcutaneously implanted osmotic minipumps (Model 2ML1) were purchased from Alzet (Palo Alto, CA).

Animals.

Healthy male and female Wistar Rats were purchased from Envigo (Indianapolis, IN). Rats had free access to rat chow and drinking water. Rats were housed two per cage under controlled temperature and humidity with 12 h :12 h dark/light cycles. The study protocols adhered to the Principles of Laboratory Animal Care (National Institute of Health publication 85-23, revised 1985) and were approved by the University at Buffalo Institutional Animal Care and Use Committee.

DEX Pharmacokinetics.

Three male rats, weighing around 310 g, and three female rats of about 280 g were first studied. DEX was infused SC through Alzet osmotic pumps at concentrations of 3 and 1.45 mg/mL at rates of 10 uL/h for 24 h in order to achieve similar steady-state plasma drug concentrations. Animals were then sacrificed, and plasma, blood (female only) as well as harvested tissues were processed for LCMS analysis of drug concentrations. A second group of male rats received a single SC dose of 2.25 mg/kg DEX. These rats were sacrificed at 9 time points (N = 3 per time point): 0.25, 0.5, 1, 2, 4, 6, 8, 12 and 24 h. In all studies, whole blood and tissues were harvested including heart, liver, spleen, lung, kidney, muscle (gastrocnemius), skin, abdominal fat, brain, bone (tibia),

and intestine. Plasma was obtained by centrifugation (2000 × g, 4°C, 15 min) using EDTA as anticoagulant (final concentration 4 mmol/L). Collected tissues were frozen in liquid nitrogen, ground to a fine powder under liquid nitrogen, and stored at -80°C until extraction.

In Vitro Blood Partitioning.

Fresh blood was collected from an untreated female Wistar rat with EDTA as anticoagulant. Part of the collected blood was centrifuged for plasma (2000 × g, 4°C, 15 min). Methanolic stocks of DEX were spiked into blank blood to yield approximately 1500, 500, 5 ng/mL concentrations and DEX was also added into blank plasma to obtain 1500 ng/mL samples. Then 150 uL aliquots of these spiked blood and plasma samples were immediately frozen for DEX quantification. The remaining samples were incubated for 60 min at 37℃. Immediately after incubation, 150 uL of all samples were transferred into microfuge tubes and frozen. These provided total DEX concentrations after incubation to assess possible DEX degradation in either blood or plasma during incubation. The remaining blood samples after incubation were spun to obtain plasma (2000 × g, 4°C, 15 min). Plasma samples were frozen and stored at -20°C for the following analysis.

Sample Preparation and DEX LC/MS Assay.

Detailed sample preparation for plasma and tissues was reported previously (Li et al., 2017; Ayyar et al., 2019b). Briefly, 100 μL 4% phosphoric acid was added to the same volume of plasma and then spiked with 10 μL of IS (D5-DEX) working solution. After vortexing and centrifugation at 13,000×g for 10 min at 10°C, supernatants were subjected to solid-phase extraction using Oasis HLB 1-cm^3 30-mg cartridges (Waters Corp.). Homogenates of tissues were prepared and drug extracted with methanol. In brief, powdered tissue was homogenized in PBS at a 6-fold dilution using a PRO-200 BIO-GEN homogenizer (ProScientific, Oxford, CT) at maximum speed setting 5 for 30 seconds. Experimental homogenates totaling 100 ul was added into 990 μL methanol and

then spiked with 10 µL of IS stocks. After vortexing and centrifugation (4°C at 14,000×g for 20 min) the supernatants were transferred to glass tubes and dried under nitrogen flow. The dried residue was reconstituted with 50 µL methanol, vortexed twice for 30 sec, and diluted with water (450 µL). Then samples (450 µL) were mixed with equal volumes of 4% phosphoric acid in microfuge tubes and underwent solid phase extraction using Oasis Prime HLB 1-cm^3 30-mg cartridges. Blood samples without dilution were directly homogenized for 30 sec at maximum speed and then were treated the same as tissue samples. The reconstitution solution for dried residue was 200 µL of acetonitrile/water (30:70, v/v). The mobile phase consisted of one eluent (acetonitrile/water (5:95 v/v) containing 0.1% formic acid) and the second (acetonitrile/water (95:5 v/v) containing 0.1% formic acid). The lower limit of quantification of DEX was 0.2 ng/ml (or ng/g) in plasma, blood and tissues. Based on extensive data obtained over decades, corticosteroids in various matrices and during freeze–thaw cycles are known to be stable and were not investigated here (Volin, 1995).

Data Analysis.

Blood to plasma ratios at each concentration was calculated by:

$$B/_P = {C_{Blood}}/{C_{Plasma}}$$

The DEX concentrations for this calculation were obtained either from the in vitro blood partitioning study or the SC infusion study in female rats.

Tissue DEX concentration data were corrected for residual blood as follows:

$$C_t = \frac{C_{t(meas)} \cdot V_{meas} - C_{pl} \cdot V_{meas} \cdot (V_{vasc}/V_t)}{V_{meas} - [V_{meas} \cdot (V_{vasc}/V_t)]} \tag{1}$$

where C_t and $C_{t(meas)}$ are the corrected and measured tissue concentrations, C_{pl} is the measured plasma concentration, V_{meas} is the measured or estimated volumes of collected tissues, V_{vasc} is the tissue vascular volume, and V_t is the tissue volume. Literature reported values were used to

9

correct tissue DEX concentrations (Bernareggi and Rowland, 1991).

Tissue partition coefficients K_p were obtained using several methods:

1. Calculation from steady-state data from the infusion study.

$$K_{P,i} = \frac{C_{i,ss}}{C_{p,ss}} \text{ (For non-eliminating organ)} \qquad (2)$$

$$K_{P,hep} = \frac{C_{hep,ss}}{C_{plasma,ss}} \cdot \left(\frac{Q_{hep} + f_{u,p} \cdot CL_{u,int}}{Q_{hep}} \right) \text{ (For liver as eliminating organ)} \qquad (3)$$

where C is the measured concentration, Q_{hep} is the hepatic blood flow, $CL_{u,int}$ is the intrinsic clearance, and subscripts indicate the tissue (i), plasma (p) and steady-state (ss).

2. Parameter estimation through PBPK modeling as described in detail below.

3. In silico K_p prediction using GastroPlus^{TM} PBPK Simulator (version 9.6.2, Simulations Plus Inc., Lancaster, CA). As described previously (Ayyar et al., 2019b), published methods (Poulin and Theil, 2002), (Berezhkovskiy, 2004), (Rodgers and Rowland, 2006) for neutral compounds were used and are listed as Methods 1-3.

PBPK Model.

Figure 1 shows the proposed PBPK model structure for DEX. Arterial and venous blood were modeled as two separate compartments and the measured blood concentrations were treated as arterial blood concentrations. This model consisted of 12 tissues including liver, kidney, lung, heart, spleen, intestine, muscle, fat, bone, skin, brain, and remainder. All organs except those mentioned were lumped into the remainder compartment. The blood flow for each organ except lung originates as arterial blood, then perfuses each organ, and converges as venous blood. In lung, blood flow is reversed. For intestine and spleen, after leaving the tissues, blood goes through the liver via the hepatic portal vein and mixes with liver artery flow upon entry into venous blood. The elimination pathway for DEX is predominantly hepatic metabolism through CYP3A pathways in

rodents (Tomlinson et al., 1997), and only free hepatic DEX is assumed to diffuse through cellular

membranes and is subject to metabolism. The rat brain K_p was assumed as 1.20 as measured in P-

gp knockout mice (Uchida et al., 2011), and bi-directional apparent permeability coefficients that

involve both passive diffusion and active efflux were employed. All physiological parameter

definitions and values are listed in Table 1. The plasma protein binding of DEX was determined

previously (Ayyar et al., 2019b) as 0.175 plasma free fraction ($f_{u,p}$) and used to calculate DEX

free fraction in liver ($f_{u,L}$) from:

$$f_{u,L} = \frac{f_{u,p}}{K_{p,L}} \qquad (4)$$

where $K_{p,L}$ is the plasma partition coefficient for liver.

The differential equations for the PBPK model are:

Venous blood:

$$V_V \cdot \frac{dC_V}{dt} = Input + R_B \cdot (Q_{liver} \cdot \frac{C_{liver}}{K_{p,liver}} + Q_{kidney} \cdot \frac{C_{kidney}}{K_{p,kidney}} + Q_{heart} \cdot \frac{C_{heart}}{K_{p,heart}} + Q_{muscle} \cdot \frac{C_{muscle}}{K_{p,muscle}} + Q_{fat} \cdot$$

$$\frac{C_{fat}}{K_{p,fat}} + Q_{bone} \cdot \frac{C_{bone}}{K_{p,bone}} + Q_{skin} \cdot \frac{C_{skin}}{K_{p,skin}} + Q_{rest} \cdot \frac{C_{rest}}{K_{p,rest}}) + Q_{brain} \cdot C_{brain,cap} - Q_{lung} \cdot C_V \qquad (5)$$

$$Q_{liver} = Q_{liver,art} + Q_{intestine} + Q_{spleen} \qquad (6)$$

Lung:

$$V_{lung} \cdot \frac{dC_{lung}}{dt} = Q_{lung} \cdot C_V - Q_{lung} \cdot \frac{R_B \cdot C_{lung}}{K_{p,lung}} \qquad (7)$$

Arterial blood:

$$V_A \cdot \frac{dC_A}{dt} = Q_{lung} \cdot \frac{R_B \cdot C_{lung}}{K_{p,lung}} - (Q_{liver,art} + Q_{kidney} + Q_{heart} + Q_{muscle} + Q_{intestine} + Q_{spleen} +$$

$$Q_{fat} + Q_{bone} + Q_{skin} + Q_{brain} + Q_{rest}) \cdot C_A \qquad (8)$$

Spleen:

$$V_{spleen} \cdot \frac{dC_{spleen}}{dt} = Q_{spleen} \cdot (C_A - \frac{R_B \cdot C_{spleen}}{K_{p,spleen}}) \qquad (9)$$

11

Intestine:

$$V_{intestine} \cdot \frac{dC_{intestine}}{dt} = Q_{intestine} \cdot (C_A - \frac{R_B \cdot C_{intestine}}{K_{p,intestine}}) \tag{10}$$

Liver:

$$V_{liver} \cdot \frac{dC_{liver}}{dt} = Q_{liver,art} \cdot C_A + Q_{spleen} \cdot \frac{R_B \cdot C_{spleen}}{K_{p,spleen}} + Q_{intestine} \cdot \frac{R_B \cdot C_{intestine}}{K_{p,intestine}} - Q_{liver} \cdot \frac{R_B \cdot C_{liver}}{K_{p,liver}} -$$

$$CL_{u,int} \cdot C_{liver} \cdot f_{u,l} \tag{11}$$

Kidney:

$$V_{kidney} \cdot \frac{dC_{kidney}}{dt} = Q_{kidney} \cdot (C_A - \frac{R_B \cdot C_{kidney}}{K_{p,kidney}}) \tag{12}$$

Heart:

$$V_{heart} \cdot \frac{dC_{heart}}{dt} = Q_{heart} \cdot (C_A - \frac{R_B \cdot C_{heart}}{K_{p,heart}}) \tag{13}$$

Adipose:

$$V_{fat} \cdot \frac{dC_{fat}}{dt} = Q_{fat} \cdot (C_A - \frac{R_B \cdot C_{fat}}{K_{p,fat}}) \tag{14}$$

Muscle:

$$V_{muscle} \cdot \frac{dC_{muscle}}{dt} = Q_{muscle} \cdot (C_A - \frac{R_B \cdot C_{muscle}}{K_{p,muscle}}) \tag{15}$$

Bone:

$$V_{bone} \cdot \frac{dC_{bone}}{dt} = Q_{bone} \cdot (C_A - \frac{R_B \cdot C_{bone}}{K_{p,bone}}) \tag{16}$$

Skin:

$$V_{skin} \cdot \frac{dC_{skin}}{dt} = Q_{skin} \cdot (C_A - \frac{R_B \cdot C_{skin}}{K_{p,skin}}) \tag{17}$$

Remainder:

$$V_{rest} \cdot \frac{dC_{rest}}{dt} = Q_{rest} \cdot (C_A - \frac{R_B \cdot C_{rest}}{K_{p,rest}}) \tag{18}$$

Brain capillary:

$$V_{brain,cap} \cdot \frac{dC_{brain,cap}}{dt} = Q_{brain} \cdot (C_A - C_{brain,cap}) - PS_{L-AL} \cdot f_{u,p} \cdot \frac{C_{brain,cap}}{R_B} + PS_{AL-L} \cdot C_{brain,} \cdot f_{u,p}/$$

$$K_{p,brain} \tag{19}$$

Brain:

$$V_{brain,} \cdot \frac{dC_{brain}}{dt} = PS_{L-AL} \cdot f_{u,p} \cdot \frac{C_{brain,cap}}{R_B} - PS_{AL-L} \cdot C_{brain,} \cdot f_{u,p}/K_{p,brain} \tag{20}$$

where V_i, Q_i, C_i and $K_{p,i}$ are volume, blood flow, DEX concentration and partition coefficient for

tissue i; R_B is blood to plasma ratio; $CL_{u,int}$ is the unbound intrinsic clearance in liver; PS_{L-AL} and

PS_{AL-L} are permeability coefficients for luminal-abluminal and abluminal-luminal in brain.

The dosing input for SC administration is:

$$Input = ka \cdot Dose \cdot F$$

The initial conditions for all differential equations are equal to 0. Bioavailability (F) was fixed to

0.86 according to previous literature (Samtani and Jusko, 2005).

After model fitting, K_p values for female rats obtained from the infusion study and

physiological parameters scaled by body weight (exponents for volume and blood flow: 1 and 0.75)

were used to simulate the plasma PK profile after the 2.25 mg/kg SC single-dose (mean body

weight 112 g). This simulated profile was overlaid with our observed data for female rats (Li et al.,

2017).

Model Fitting.

The tissue partition coefficients for all harvested tissues (K_p), two brain permeability

coefficients (PS), SC absorption rate constant (k_a), and hepatic intrinsic clearance ($CL_{u,int}$) were

estimated. All fittings and simulations were implemented using ADAPT 5 (Biomedical

Simulations Resource, University of Southern California, Los Angeles, CA) using maximum

likelihood estimation. The ADAPT code for modeling our data is provided in the Supplemental

Materials. The model was evaluated based on Akaike Information Criterion (AIC), visual

inspection of the fitted profiles and CV% of parameter estimates. The variance model was:

$$V_i = (\sigma_1 + \sigma_2 \cdot Y_i)^2 \tag{21}$$

where V_i represents the variance of the ith data point, Y_i is the ith model prediction, and σ_1 and σ_2

are variance model parameters. All figures were created using GraphPad Prism 7.04 (GraphPad

Software, La Jolla, CA).

Results

Blood cell partitioning

As shown in Figure 2 the DEX blood to plasma ratios (*B/P*) based on female rat SC infusion and in vitro partitioning were calculated to be 0.727 (SD = 0.07, n = 3) and 0.723 (SD = 0.08, n = 3) with combined *B/P* value of 0.725 (SD = 0.08, n = 6). The lower DEX concentration in blood compared with plasma appears to be due to protein binding (82.5%, to be shown). The average *B/P* obtained from the male rat SC bolus study was 0.664, which was slightly smaller than the female.

Whole-body pharmacokinetics of DEX

Figure 3 shows measured and fitted time-course PK profiles of DEX after single SC dosing in blood and tissues. Generally, the current model captures the tissue PK well with slight overestimation for muscle. The delayed peak DEX concentration in brain necessitated the incorporation of permeability-limited entry and transporter-mediated efflux with two different permeability coefficients.

The DEX K_p for each tissue as well as other relevant parameters were obtained from PBPK modeling of male SC bolus data (Table 2). The intercept and slope for the variance model were 1.39 and 0.22. All parameters were estimated with good precision with CV% < 50%. The K_p values for most tissues are around 1. However, the K_p values are 6.76 for liver and 1.51 for kidney, indicating extensive partitioning of DEX in liver and above-average partitioning in kidney. In adipose tissue, the K_p value obtained (0.15) was surprisingly low. Our model-fitted K_p values were very close to those calculated from our steady-state infusion study in male rats as shown in Table 2. The two estimated permeability coefficients showed a large difference (1.46 vs 24.3), which indicates significant contribution of active efflux from the brain.

15

Comparing results from males and females in the infusion study, K_p values were similar except for modest differences for lung, intestine, kidney, liver, and possibly fat. Lung had a greater K_p in females than males (0.69 ± 0.09 vs. 0.50 ± 0.06), and males had greater K_p values (e.g. 5.06 ± 0.56 vs. 4.10 ± 0.56 in liver) for the other four tissues. The measured liver K_p for both sexes from the infusion studies were 4.55 (male) and 3.76 (female) without correction for metabolism (Eq. 3). As expected, the corrected K_p values increased to 5.06 and 4.10. As illustrated in Table 2, the in vivo K_p values for most tissues showed distinct differences from in silico values obtained using the three calculation methods. Figure 4 shows a simulated DEX plasma PK profile in female rats illustrating that model predictions are in good agreement with measured plasma concentrations except for the last time point.

Rat hematocrit (HCT) values were reported as 0.40 (male) and 0.37 (female) (Probst et al., 2006) and we obtained mean DEX *B/P* values of 0.664 (male) and 0.725 (female). If we assume that only free DEX in plasma partitions into blood cells and red blood cells (RBC) are the predominant cells in blood, *B/P* could be obtained from:

$$\frac{C_{Blood}}{C_{Plasma}} = \frac{C_{Plasma} \cdot f_{u,p} \cdot V_{Blood} \cdot HCT + C_{Plasma} \cdot V_{Blood} \cdot (1 - HCT)}{V_{Blood} \cdot C_{Plasma}}$$

$$= f_{u,p} \cdot HCT + (1 - HCT) \qquad (22)$$

where $f_{u,p}$ is the DEX plasma free fraction (0.175). The calculated *B/P* are 0.670 (male) and 0.695 (female), which are similar to in vivo values. The GastroPlusTM predicted *B/P* of 0.88 was slightly greater than experimental values. These findings suggest that limited entry of DEX into RBC may be attributed to the moderate plasma protein binding.

Discussion

The purposes of the current study were to assess the tissue distribution of DEX in male and female rats and to develop a PBPK model based on experimental data. Most PBPK studies do not address sex differences and in silico prediction methods do not take this factor into account. An extensive assessment of the human PK of DEX and betamethasone with a focus on the role of human pregnancy was carried out recently (Ke and Milad, 2019). This included PBPK simulations using the Simcyp Simulator V17 R1. Their tissue distribution properties of DEX were likely generated using the same or similar in silico predictions that we have employed. It is not possible to anticipate whether the unusual Kp values that we observed in some tissues and the role of the brain P-gp transport would be present in humans. Our study involved dosing by SC injection instead of oral or IV administration as offering more reliable absorption, ensuring dosing accuracy, producing less animal stress, and to relate the data to our previous work (Earp et al., 2008; Li et al, 2017).

The distribution of DEX into RBC is similar to that for prednisolone. Previous studies in rabbits showed that prednisolone RBC concentrations were equal to free plasma concentrations indicating a similar role of protein binding (Khalafallah and Jusko, 1984). In addition, the endogenous glucocorticoid corticosterone also exhibited a low B/P ratio (0.55) in zebra finches (Taves et al., 2010)

As shown in Table 2, some of the tissues have Kp values greater than 1, indicating higher concentrations of DEX in those tissues than plasma. However, for adipose tissue, the K_p value is unexpectedly much smaller than 1. DEX was expected to partition somewhat into adipose tissue due to its moderate lipophilic nature (LogP = 1.83). A similar phenomenon was observed for prednisolone in rabbits (Khalafallah and Jusko, 1984) and rats (unpublished). For brain tissue, the

K_p from SC infusion data was estimated to be 0.09, although DEX can readily diffuse through cell membranes and the blood-brain barrier. However, DEX is a substrate for p-glycoprotein transporters (Ueda et al., 1992; Schinkel et al., 1995) and its brain distribution was affected by P-gp in mice as seen with the extremely small K_p value calculated from infusion studies (Uchida et al., 2011). Therefore, the efflux of DEX from brain mediated by the highly expressed P-gp in the blood-brain barrier was assumed to occur and was incorporated into our PBPK model. Interestingly, the ratio of the two permeability parameters is 16.6, similar to the literature reported flux ratio for DEX (14.7) using LLC-PK1/L-mdr1a cell monolayers (Uchida et al., 2011).

After correction for tissue metabolism, the liver K_p was 6.76, which suggests appreciable liver partitioning and binding and is in agreement with liver distribution data for other corticosteroids, such as methylprednisolone (Ayyar et al., 2019b) and prednisolone (unpublished). In silico methods underpredict the liver K_p at least 4-fold. These methods mainly assume that tissue distribution was governed by composition differences between tissue and plasma in terms of neutral/phospho- lipids and water with consideration of binding to albumin and lipoprotein. However, DEX binds to glucocorticoid receptors, which are highly expressed in the liver and this high affinity binding may help retain DEX in the liver and partially contribute to the liver Kp. At the same time, evidence for the presence of a glucocorticoid-responsive site in highly purified rat liver plasma membranes was found (Lackner et al., 1998), which was able to mediate active uptake of DEX, possibly contributing to the liver Kp and in vivo vs in silico differences. In the remaining tissues, such as intestine, muscle, lung and heart, DEX partitioning was less compared to liver and kidney. In addition, the K_p in skin was 0.40, indicating modest distribution.

Tissue partitioning parameters obtained from male and female rats were similar in some tissues, differing in others within 1.6-fold. Causes of these differences remained to be determined.

By using female K_p values and scaling the physiological parameters for the difference in body sizes, we captured DEX plasma PK profiles in female rats very well (Figure 4), which further supports our analysis approach.

In silico methods are widely applied in PK modeling to obtain some key parameter values that are difficult to directly measure. However, our current results suggest that, while most worked well, differences exist between in vivo and in silico results, especially for the elimination organs. Therefore, caution is needed in adopting in silico values alone; ideally joint application of in vivo, in silico, and in vitro approaches in PK investigations would increase confidence in results.

Females have slightly smaller clearance values than males (Table 2). This was also found for methylprednisolone in rats (Ayyar et al, 2019a). It is expected that, as a CYP3A substrate, any sex differences should be modest (Gandhi et al., 2004). No publications for DEX were found, although methylprednisolone exhibits higher clearances in women (Lew et al., 1993),

A potential limitation of our current study involved brain distribution. The P-gp mediated efflux of DEX was combined with passive diffusion using linear permeability coefficients because of limited information and inability of modeling to discern a low K_p from transporter efflux. Active transport often exhibits a maximal capacity and affinity. However, in vivo substrate concentrations are usually low relative to transport mechanisms leading to expectations of linear brain distribution (Kalvass et al., 2013).

From this investigation on tissue distribution and whole-body PK, it is evident that DEX can easily enter all major tissues and subsequently elicit biological effects upon binding to ubiquitously expressed glucocorticoid receptors. DEX distribution into non-target tissues can also the trigger undesired adverse effects. This model may help predict DEX concentrations across different tissues for better understanding of GC pharmacodynamics.

Conclusions

Our PBPK model well describes the experimentally determined tissue and plasma DEX PK profiles in rats. The apparent P-gp mediated transport across the BBB describes DEX efflux from brain tissue that resulted in a very low measured partition coefficient. Our current model can serve for further investigation of DEX tissue distribution in rats as the PK driving force for receptor-mediated PD effects in various tissues. Slight sex differences were found for DEX tissue distribution and clearance. Knowledge gained in this study may be translatable to other species.

Authorship Contributions

Participated in research design: Song, Sun, DuBois, Almon, Jusko

Conducted experiments：Song, Sun, DuBois

Performed data analysis：Song, Sun, DuBois, Almon, Meng, Jusko

Wrote or contributed to the writing of the manuscript: Song, Sun, DuBois, Jusko

References

Ayyar VS, DuBois DC, Nakamura T, Almon RR, and Jusko WJ (2019a) Modeling corticosteroid pharmacokinetics and pharmacodynamics, Part II: Sex differences in methylprednisolone pharmacokinetics and corticosterone suppression. *J Pharmacol Exp Ther* **370:**327-336.

Ayyar VS, Song D, DuBois DC, Almon RR, and Jusko WJ (2019b) Modeling corticosteroid pharmacokinetics and pharmacodynamics, Part I: Determination and prediction of dexamethasone and methylprednisolone tissue binding in the rat. *J Pharmacol Exp Ther* **370:**318-326.

Baschant U, Lane NE, and Tuckermann J (2012) The multiple facets of glucocorticoid action in rheumatoid arthritis. *Nat Rev Rheumatol* **8:**645-655.

Berezhkovskiy LM (2004) Volume of distribution at steady state for a linear pharmacokinetic system with peripheral elimination. *J Pharm Sci* **93:**1628-1640.

Bernareggi A and Rowland M (1991) Physiologic modeling of cyclosporin kinetics in rat and man. *J Pharmacokinet Biopharm* **19:**21-50.

Bischoff KB, Dedrick RL, and Zaharko DS (1970) Preliminary model for methotrexate pharmacokinetics. *J Pharm Sci* **59:**149-154.

Bischoff KB, Dedrick RL, Zaharko DS, and Longstreth JA (1971) Methotrexate pharmacokinetics. *J Pharm Sci* **60:**1128-1133.

Cato AC, Nestl A, and Mink S (2002) Rapid actions of steroid receptors in cellular signaling pathways. *Sci STKE* **2002:**re9.

Earp JC, Pyszczynski NA, Molano DS, and Jusko WJ (2008) Pharmacokinetics of dexamethasone in a rat model of rheumatoid arthritis. *Biopharm Drug Dispos* **29:**366-372.

Gandhi M, Aweeka F, Greenblatt RM, and Blaschke TF (2004) Sex differences in
pharmacokinetics and pharmacodynamics. *Annu Rev Pharmacol Toxicol* **44:** 499-523.

Jones H and Rowland-Yeo K (2013) Basic concepts in physiologically based pharmacokinetic
modeling in drug discovery and development. *CPT Pharmacometrics Syst Pharmacol*
2:e63.

Jones HM, Chen Y, Gibson C, Heimbach T, Parrott N, Peters SA, Snoeys J, Upreti VV, Zheng
M, and Hall SD (2015) Physiologically based pharmacokinetic modeling in drug
discovery and development: a pharmaceutical industry perspective. *Clin Pharmacol Ther*
97:247-262.

Kadmiel M and Cidlowski JA (2013) Glucocorticoid receptor signaling in health and disease.
Trends Pharmacol Sci **34:**518-530.

Kalvass JC, Polli JW, Bourdet DL, Feng B, Huang SM, Liu X, Smith QR, Zhang LK, Zamek-
Gliszczynski M J (2013) Why clinical modulation of efflux transport at the human blood-
brain barrier is unlikely: The ITC evidence-based position. *Clin Pharmacol Ther*, **94:** 80-
94.

Ke AB and Milad MA (2019) Evaluation of maternal drug exposure following the administration
of antenatal corticosteroids during late pregnancy using physiologically-based
pharmacokinetic modeling. *Clin Pharmacol Ther*, **106:** 164-173.

Khalafallah N and Jusko WJ (1984) Tissue distribution of prednisolone in the rabbit. *J
Pharmacol Exp Ther* **229:**719-725.

Lackner C, Daufeldt S, Wildt L, and Alléra A (1998) Glucocorticoid-recognizing and -effector
sites in rat liver plasma membrane. Kinetics of corticosterone uptake by isolated

membrane vesicles. III. Specificity and stereospecificity. *J Steroid Biochem Mol Biol* **64:** 69-82.

Lew KH, Ledwig EA, Milad MA, Donovan K, Middleton E Jr, Ferry JJ, and Jusko WJ (1993) Gender-based effects on methylprednisolone pharmacokinetics and pharmacodynamics. *Clin Pharmacol Ther*, **54:** 402-414.

Li X, DuBois DC, Song D, Almon RR, Jusko WJ, and Chen X (2017) Modeling combined immunosuppressive and anti-inflammatory effects of dexamethasone and naproxen in rats predicts the steroid-sparing potential of naproxen. *Drug Metab Dispos* **45:**834-845.

Losel R and Wehling M (2003) Nongenomic actions of steroid hormones. *Nat Rev Mol Cell Biol* **4:**46-56.

Napier C and Pearce SH (2014) Current and emerging therapies for Addison's disease. *Curr Opin Endocrinol Diabetes Obes* **21:**147-153.

Oakley RH and Cidlowski JA (2011) Cellular processing of the glucocorticoid receptor gene and protein: new mechanisms for generating tissue-specific actions of glucocorticoids. *J Biol Chem* **286:**3177-3184.

Poulin P and Theil FP (2002) Prediction of pharmacokinetics prior to in vivo studies. II. Generic physiologically based pharmacokinetic models of drug disposition. *J Pharm Sci* **91:**1358-1370.

Probst RJ, Lim JM, Bird DN, Pole GL, Sato AK, and Claybaugh JR (2006) Gender differences in the blood volume of conscious Sprague-Dawley rats. *J Am Assoc Lab Anim Sci* **45:**49-52.

Rhen T and Cidlowski JA (2005) Antiinflammatory action of glucocorticoids--new mechanisms for old drugs. *N Engl J Med* **353:**1711-1723.

Rodgers T and Rowland M (2006) Physiologically based pharmacokinetic modelling 2: predicting the tissue distribution of acids, very weak bases, neutrals and zwitterions. *J Pharm Sci* **95:**1238-1257.

Sager JE, Yu J, Ragueneau-Majlessi I, and Isoherranen N (2015) Physiologically based pharmacokinetic (PBPK) modeling and simulation approaches: A systematic review of published models, applications, and model verification. *Drug Metab Dispos* **43:**1823-1837.

Samtani MN and Jusko WJ (2005) Comparison of dexamethasone pharmacokinetics in female rats after intravenous and intramuscular administration. *Biopharm Drug Dispos* **26:**85-91.

Samtani MN, Pyszczynski NA, DuBois DC, Almon RR, and Jusko WJ (2006) Modeling glucocorticoid-mediated fetal lung maturation: I. Temporal patterns of corticosteroids in rat pregnancy. *J Pharmacol Exp Ther* **317:**117-126.

Schinkel AH, Wagenaar E, van Deemter L, Mol CA, and Borst P (1995) Absence of the mdr1a P-Glycoprotein in mice affects tissue distribution and pharmacokinetics of dexamethasone, digoxin, and cyclosporin A. *J Clin Invest* **96:**1698-1705.

Shah DK and Betts AM (2012) Towards a platform PBPK model to characterize the plasma and tissue disposition of monoclonal antibodies in preclinical species and human. *J Pharmacokinet Pharmacodyn* **39:**67-86.

Song D, DuBois DC, Almon RR, and Jusko WJ (2018) Modeling sex differences in anti-inflammatory effects of dexamethasone in arthritic rats. *Pharm Res* **35:**203.

Taves MD, Schmidt KL, Ruhr IM, Kapusta K, Prior NH, and Soma KK (2010) Steroid concentrations in plasma, whole blood and brain: effects of saline perfusion to remove blood contamination from brain. *PloS one* **5:**e15727.

Tomlinson ES, Maggs JL, Park BK, and Back DJ (1997) Dexamethasone metabolism in vitro: species differences. *J Steroid Biochem Mol Biol* **62:**345-352.

Uchida Y, Ohtsuki S, Kamiie J, and Terasaki T (2011) Blood-brain barrier (BBB) pharmacoproteomics: reconstruction of in vivo brain distribution of 11 P-glycoprotein substrates based on the BBB transporter protein concentration, in vitro intrinsic transport activity, and unbound fraction in plasma and brain in mice. *J Pharmacol Exp Ther* **339:**579-588.

Ueda K, Okamura N, Hirai M, Tanigawara Y, Saeki T, Kioka N, Komano T, and Hori R (1992) Human P-glycoprotein transports cortisol, aldosterone, and dexamethasone, but not progesterone. *J Biol Chem* **267:**24248-2425P (1995) High-performance liquid chromatographic analysis of corticosteroids. *J Chromatogr B Biomed Appl* **671:**319-340.

Zhuang X and Lu C (2016) PBPK modeling and simulation in drug research and development. *Acta Pharm Sin B* **6:**430-440.

Footnotes

Table 1. Physiological parameters of tissues in a 310 g male rat

Tissue	Volume (V, mL)	Blood Flow (Q, mL/h)
Lung	1.11[a]	5779[b]
Brain	1.51[a]	128[b]
Heart	0.92[a]	297[b]
Intestine	8.61[b]	1091[b]
Spleen	0.42[a]	351[b]
Kidney	1.82[a]	716[b]
Muscle	134.5[b]	1815[b]
Liver Artery	11.3[a]	41.4[b]
Skin	55.1[b]	392[b]
Bone	22.8[b]	120[b]
Fat	36.4[b]	440[b]
Arterial Blood	6.08[b]	5779[b]
Venous Blood	12.2[b]	5779[b]
Rest of body	17.2[c]	387[c]

[a]: Experiment value

[b]: From (Shah and Betts, 2012)

[c]: Calculated value (1. assuming 1 ng/mL tissue density, Volume for rest of body = body weight – summation of volume for listed tissues; 2. Blood flow for rest of body = cardiac output - summation of blood flow for listed tissues)

Table 2. Summary of DEX pharmacokinetic parameters

Tissue	PBPK	Male Infusion[c]	Female Infusion[c]	Method 1	Method 2	Method 3
$K_{p,Lung}$	0.55[a]	0.50 ± 0.06	0.69 ± 0.09	1.4	0.8	0.59
$K_{p,Brain}$	1.20[b]	0.06[b] ± 0.003	0.10[b] ± 0.02	2.53	1.16	0.85
$K_{p,Heart}$	0.86[a]	0.84 ± 0.20	0.85 ± 0.06	1.09	0.68	0.48
$K_{p,Intestine}$	0.79[a]	0.82 ± 0.14	0.52 ± 0.04	NA[d]	NA[d]	NA[d]
$K_{p,Spleen}$	0.64[a]	0.63 ± 0.09	0.46 ± 0.07	0.87	0.61	0.45
$K_{p,Kidney}$	1.51[a]	1.24 ± 0.05	1.05 ± 0.05	1.21	0.72	0.50
$K_{p,Muscle}$	0.58[a]	0.49 ± 0.05	0.42 ± 0.04	0.89	0.61	0.33
$K_{p,Liver}$	6.76[a]	5.06 ± 0.56	4.10 ± 0.56	1.26	0.71	0.53
$K_{p,Skin}$	0.40[a]	0.30 ± 0.08	0.35 ± 0.03	1.46	0.75	0.55
$K_{p,Bone}$	0.23[a]	0.19 ± 0.03	0.16 ± 0.01	NA[e]	NA[e]	NA[e]
$K_{p,Fat}$	0.15[a]	0.16 ± 0.01	0.10 ± 0.01	1.37	0.83	0.83
$K_{p,Rest}$	1 (Fix)					

ka	SC absorption rate constant (h^{-1})		1.87[a]
$CL_{u,int}$	Hepatic intrinsic clearance (mL/h)		404.4[a]
PS_{AL-L}	Brain abluminal to luminal permeability coefficient (mL/h)		24.3[a]
PS_{L-AL}	Brain luminal to abluminal permeability coefficient (mL/h)		1.46[a]
CL	Total plasma clearance (mL/h/kg)		197.9 (SD = 16.4, male)[c]
			177.6 (SD = 26.0, female)[c]

[a]: Estimated parameters with CV% < 50% in PBPK model

[b]: Due to active transport, only an apparent K_p can be calculated from steady-state data and fixed

to 1.2 as found in mice (Uchida et al., 2011)

[c]: Calculated based on male and female SS infusion study with n = 3 (SD provided)

[d]: Tissues associated with GI tract were lumped together

[e]: Different bone marrow values were listed separately in software
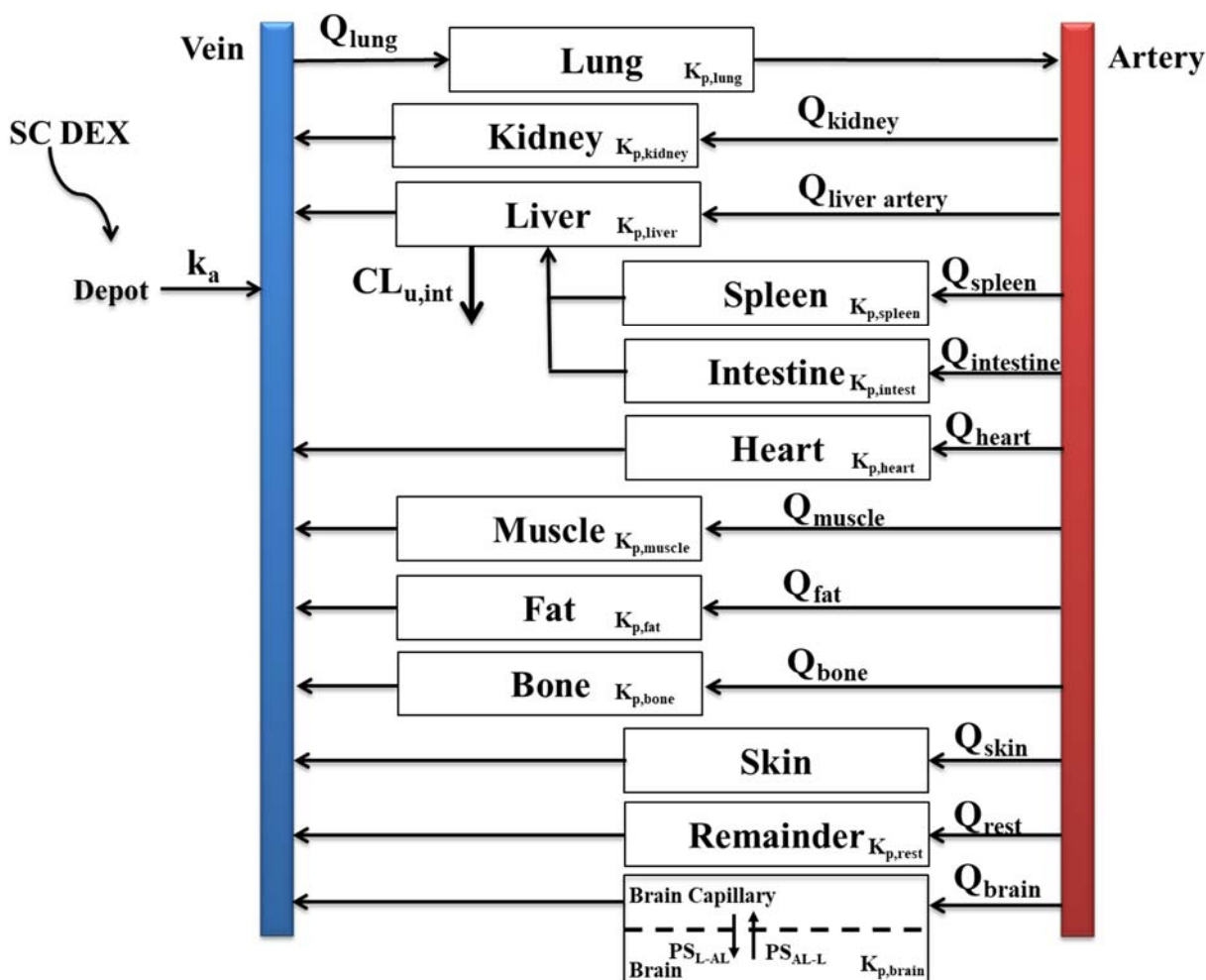
Figure 1. Schematic of the full PBPK model structure for DEX. Parameters and symbols are defined in the text and tables. Lines with arrows indicate blood flows and drug transport. Each box represents one tissue compartment as indicated by the label.
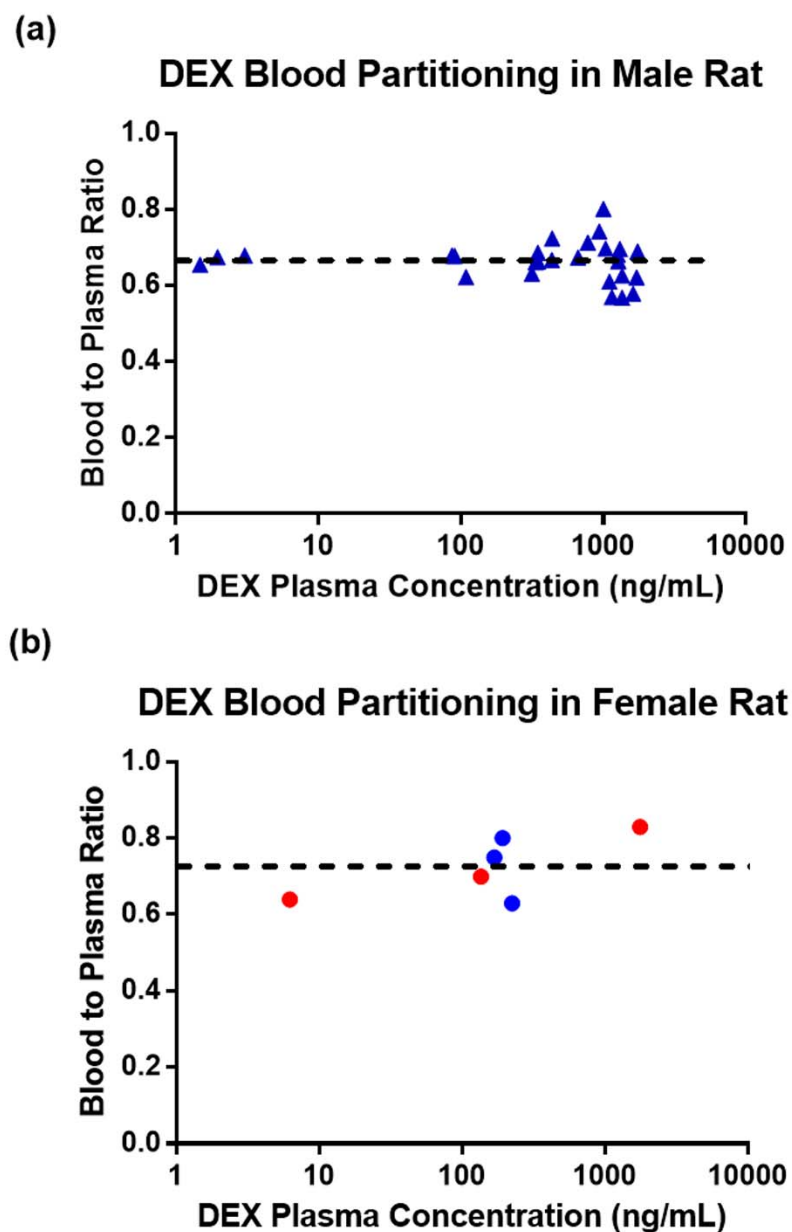
Figure 2. DEX blood to plasma ratio versus corresponding plasma concentrations in male and female rats. Blue triangles are ratios calculated from the SC bolus study in male rats. Red dots indicate the ratio calculated from the in vitro blood cell partitioning study and blue dots are ratios calculated from the SC infusion study in female rats. The dashed line shows the mean value of all points.
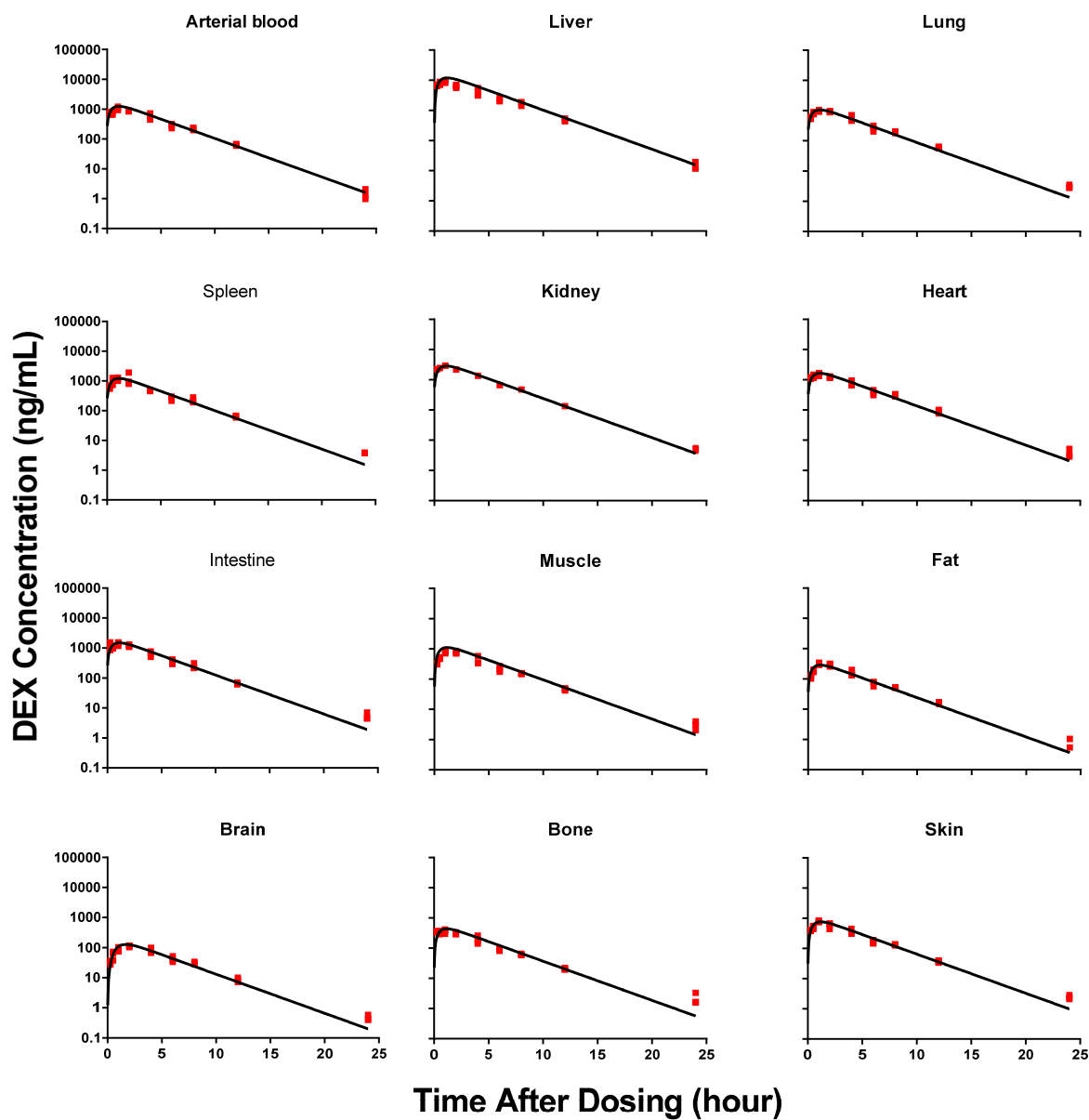
Figure 3. DEX concentration-time profiles across all tissues after 2.25 mg/kg SC DEX single dosing. Measured DEX concentrations in blood and tissues are indicated by red squares and black solid lines show the model fitting.

DEX Plasma PK in Female Rats
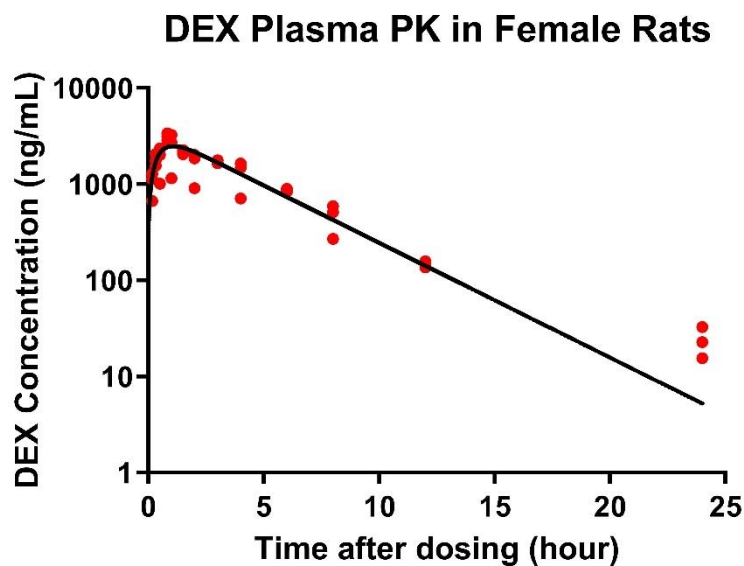
Figure 4. PBPK model-predicted plasma DEX concentrations after 2.25 mg/kg SC dosing in female rats. Black solid line shows the model prediction and red dots are measured concentrations.

Physiologically-Based Pharmacokinetics of Dexamethasone in Rats

Dawei Song[1#], Le Sun[1#], Debra C DuBois [1,3], Richard R Almon [1,3], Shengnan Meng [2], William J Jusko [1]

[1] Department of Pharmaceutical Sciences, School of Pharmacy and Pharmaceutical Sciences, State University of New York at Buffalo, Buffalo, NY, 14214, USA

[2] Department of Pharmaceutics, School of Pharmacy, China Medical University, Shenyang 110122, China

[3] Department of Biological Sciences, State University of New York at Buffalo, Buffalo, NY, 14260, USA

[#] Authors have contributed equally to these studies

Supplemental Material: ADAPT 5 Code for DEX PBPK Modeling

```fortran
***************************************************************
C                        ADAPT                         *
C                      Version 5                        *
C***************************************************************
C                                                       *
C                        MODEL                          *
C                                                       *
C    This file contains Fortran subroutines into which the user   *
C    must enter the relevant model equations and constants.       *
C    Consult the User's Guide for details concerning the format for *
C    entered equations and definition of symbols.       *
C                                                       *
C       1. Symbol-  Parameter symbols and model constants   *
C       2. DiffEq-  System differential equations       *
C       3. Output-  System output equations             *
C       4. Varmod-  Error variance model equations       *
C       5. Covmod-  Covariate model equations (ITS,MLEM)  *
C       6. Popinit- Population parameter initial values (ITS,MLEM) *
C       7. Prior -  Parameter mean and covariance values (ID,NPD,STS) *
C       8. Sparam-  Secondary parameters                 *
C       9. Amat  -  System state matrix                  *
C                                                       *
C***************************************************************


C#################################################################C

        Subroutine SYMBOL
        Implicit None

        Include 'globals.inc'
        Include 'model.inc'


CC
C-------------------------------------------------------------C
C   Enter as Indicated                                        C
C----c-------------------------------------------------------C

        NDEqs   =  16    ! Enter # of Diff. Eqs.
        NSParam =  19    ! Enter # of System Parameters.
        NVparam =  2     ! Enter # of Variance Parameters.
        NSecPar =  0     ! Enter # of Secondary Parameters.
        NSecOut =  0     ! Enter # of Secondary Outputs (not used).
        Ieqsol  =  1     ! Model type: 1 - DIFFEQ, 2 - AMAT, 3 - OUTPUT only.
        Descr   = ' full-PBPK '
CC
C-------------------------------------------------------------C
C   Enter Symbol for Each System Parameter (eg. Psym(1)='Kel')  C
C----c-------------------------------------------------------C


        Psym(1)='Kp_kidney'
```

```fortran
        Psym(2)='Kp_liver'
        Psym(3)='Kp_spleen'
        Psym(4)='Kp_heart'
        Psym(5)='Kp_lung'
        Psym(6)='Kp_muscle'
        Psym(7)='Kp_intestine'
        Psym(8)='Kp_fat'
        Psym(9)='Kp_bone'
        Psym(10)='Kp_skin'
        Psym(11)='Kp_rest'
        Psym(12)='Kp_brain'
        Psym(13)='Ka'
        Psym(14)='CLint'
        Psym(15)='F'
        Psym(16)='fu'
        Psym(17)='PS1'
        Psym(18)='PS2'
        Psym(19)='BP'

CC
C-------------------------------------------------------------------C
C   Enter Symbol for Each Variance Parameter {eg: PVsym(1)='Sigma'}   C
C----c--------------------------------------------------------------C
        PVsym(1)='sigma'
        PVsym(2)='intercept'

CC
C-------------------------------------------------------------------C
C   Enter Symbol for Each Secondary Parameter {eg: PSsym(1)='CLt'}    C
C----c--------------------------------------------------------------C


C-------------------------------------------------------------------C
C-------------------------------------------------------------------C
C
        Return
        End

C################################################################C

        Subroutine DIFFEQ(T,X,XP)
        Implicit None

        Include 'globals.inc'
        Include 'model.inc'

        Real*8 T,X(MaxNDE),XP(MaxNDE)
        Real*8 ka, F, CLint, PS1, PS2, fu, BP
        Real*8 Kp_liver, Kp_rest, Kp_lung
        Real*8 Kp_spleen, Kp_intestine, Kp_kidney, Kp_muscle, Kp_fat
        Real*8 Kp_heart, Kp_brain, Kp_bone, Kp_skin
        Real*8 Q_liver_a, Q_rest, Q_lung, Q_bone, Q_skin,Q_spleen
```

```fortran
      Real*8 Q_intestine,Q_kidney,Q_heart,Q_muscle, Q_fat,Q_brain
      Real*8 V_spleen,V_intestine, V_kidney,CLeff
      Real*8 V_heart,V_muscle, V_fat, V_brain, V_skin, V_bone
      Real*8 V_br_cap, V_liver, V_rest, V_V, V_A, V_lung

CC
C------------------------------------------------------------------C
C   Enter Differential Equations Below  {e.g.   XP(1) = -P(1)*X(1) }    C
C----c-------------------------------------------------------------C
          Kp_kidney=P(1)
          Kp_liver=P(2)
          Kp_spleen=P(3)
          Kp_heart=P(4)
          Kp_lung=P(5)
          Kp_muscle=P(6)
          Kp_intestine=P(7)
          Kp_fat=P(8)
          Kp_bone=P(9)
          Kp_skin=P(10)
          Kp_rest=P(11)
          Kp_brain=P(12)

          Ka = P(13) ! Absorption rate constant
          CLint= P(14) ! Liver unbound intrinsic clearance
          F=P(15) ! Bioavailability
          fu=P(16) ! Plasma free fraction
          PS1=P(17) ! luminal to abluminal permeability coefficient
          PS2=P(18) ! abluminal to luminal permeability coefficient
          BP=P(19) ! Blood to plasma ratio

          ! Tissue volume (mL)
          V_lung=  1.11
          V_brain= 1.51
          V_heart= 0.92
          V_intestine= 8.61 ! small + large intestine
          V_spleen=  0.42
          V_kidney=  1.82
          V_muscle= 134.53
          V_liver= 11.32
          V_skin= 55.13
          V_bone= 22.81
          V_fat= 36.42
          V_A= 6.08 ! artery
          V_V= 12.16 ! vein
          V_rest= 17.17
          V_br_cap= 0.0206 ! brain vascular space


          ! Blood flow was used to describe the flow rate to each tissues (mL/h)
          Q_lung= 5779
          Q_brain= 128
          Q_heart= 297
```

```fortran
      Q_intestine= 1091
      Q_spleen= 351
      Q_kidney= 716
      Q_muscle= 1815
      Q_liver_a= 41.4 ! Hepatic artery flow
      Q_skin=  392
      Q_bone= 120
      Q_fat= 440
      Q_rest= 387
   ! SC dosing depot amount mg
      XP(1)=-ka*X(1) ! no need to add F here because this is dosing depot
   ! Liver ng/mL
      XP(2)=(Q_liver_a*X(5)+Q_spleen*X(7)*BP/Kp_spleen+
1      Q_intestine*X(8)*BP/Kp_intestine-CLint*fu/Kp_liver*X(2)-
1     (Q_liver_a+Q_spleen+Q_intestine)*X(2)*BP/Kp_liver)/V_liver
   ! Remainder
      XP(3)=(X(5)-X(3)*BP/Kp_rest)*Q_rest/V_rest
   ! Venous
      XP(4)=(ka*X(1)*F+
1         (Q_liver_a+Q_spleen+Q_intestine)*X(2)*BP/Kp_liver+
1         Q_rest*X(3)*BP/Kp_rest+Q_kidney*X(9)*BP/Kp_kidney+
1         Q_heart*X(10)*BP/Kp_heart+Q_muscle*X(11)*BP/Kp_muscle+
1         Q_fat*X(12)*BP/Kp_fat+Q_brain*X(16)+
1         Q_bone*X(14)*BP/Kp_bone+Q_skin*X(15)*BP/Kp_skin
1         -Q_lung*X(4))/V_V
   ! Arterial
      XP(5)=(Q_lung*X(6)*BP/Kp_lung-Q_lung*X(5))/V_A
   ! Lung
      XP(6)=(Q_lung*X(4)-Q_lung*X(6)*BP/Kp_lung)/V_lung
   ! Spleen
      XP(7)=Q_spleen*(X(5)-X(7)*BP/Kp_spleen)/V_spleen
   ! Intestine
      XP(8)=Q_intestine*(X(5)-X(8)*BP/Kp_intestine)/V_intestine
   ! Kidney
      XP(9)=Q_kidney*(X(5)-X(9)*BP/Kp_kidney)/V_kidney
   ! Heart
      XP(10)=Q_heart*(X(5)-X(10)*BP/Kp_heart)/V_heart
   ! Muscle
      XP(11)=Q_muscle*(X(5)-X(11)*BP/Kp_muscle)/V_muscle
   ! Fat
      XP(12)=Q_fat*(X(5)-X(12)*BP/Kp_fat)/V_fat
   ! Bone
      XP(14)=Q_bone*(X(5)-X(14)*BP/Kp_bone)/V_bone
   ! Skin
      XP(15)=Q_skin*(X(5)-X(15)*BP/Kp_skin)/V_skin
   ! Brain
      XP(13)=(PS1*(fu/BP)*X(16)-PS2*fu*X(13)/Kp_brain)/V_brain
   ! Brain capillary (Blood)
      XP(16)=Q_brain*(X(5)-X(16))/V_br_cap
1            +PS2*fu/Kp_brain*X(13)/V_br_cap
1            -PS1*(fu/BP)*X(16)/V_br_cap
```

```fortran
C------------------------------------------------------------------C
C------------------------------------------------------------------C
C
      Return
      End

C##################################################################C

      Subroutine OUTPUT(Y,T,X)
      Implicit None

      Include 'globals.inc'
      Include 'model.inc'

      Real*8 Y(MaxNOE),T,X(MaxNDE)
      Real*8 Ka, CLint, Kp_liver, Kp_rest, Kp_lung, V_liver, V_rest
      Real*8 V_V, V_A, V_lung, Q_liver, Q_rest, Q_lung, Kp_spleen
      Real*8 V_spleen, Q_spleen, Kp_intestine, V_intestine
      Real*8 Q_intestine, Kp_kidney, V_kidney, Q_kidney, Kp_heart
      Real*8 V_heart, Q_heart, Kp_muscle, V_muscle, Q_muscle, Kp_fat
      Real*8 V_fat, Q_fat, Kp_brain, V_brain, Q_brain, Kp_bone
      Real*8 V_bone, Q_bone, Kp_skin, V_skin, Q_skin, F, fu, BP,CLeff

CC
C------------------------------------------------------------------C
C   Enter Output Equations Below   {e.g.   Y(1) = X(1)/P(2) }      C
C----c-------------------------------------------------------------C
          Y(1)=X(5)  ! Artery blood
          Y(2)=X(2)  ! Liver
          Y(3)=X(6)  ! Lung
          Y(4)=X(7)  ! Spleen
          Y(5)=X(8)  ! Intestine
          Y(6)=X(9)  ! Kidney
          Y(7)=X(10)  ! Heart
          Y(8)=X(11)  ! Muscle
          Y(9)=X(12)  ! Fat
          Y(10)=X(13)  ! Brain
          Y(11)=X(14)  ! Bone
          Y(12)=X(15)  ! Skin



C------------------------------------------------------------------C
C------------------------------------------------------------------C
C
      Return
      End

C##################################################################C
Subroutine VARMOD(V,T,X,Y)
      Implicit None

      Include 'globals.inc'
```

```fortran
      Include 'model.inc'

      Real*8 V(MaxNOE),T,X(MaxNDE),Y(MaxNOE)
      Real*8 sigma, intercept

CC
C------------------------------------------------------------------C
C   Enter Variance Model Equations Below                           C
C        {e.g.  V(1) = (PV(1) + PV(2)*Y(1))**2 }                   C
C----c-------------------------------------------------------------C
      sigma = PV(1)
      intercept = PV(2)
      V(1)  = (intercept + sigma*Y(1))**2
      V(2)  = (intercept + sigma*Y(2))**2
      V(3)  = (intercept + sigma*Y(3))**2
      V(4)  = (intercept + sigma*Y(4))**2
      V(5)  = (intercept + sigma*Y(5))**2
      V(6)  = (intercept + sigma*Y(6))**2
      V(7)  = (intercept + sigma*Y(7))**2
      V(8)  = (intercept + sigma*Y(8))**2
      V(9)  = (intercept + sigma*Y(9))**2
      V(10) = (intercept + sigma*Y(10))**2
      V(11) = (intercept + sigma*Y(11))**2
      V(12) = (intercept + sigma*Y(12))**2


C------------------------------------------------------------------C
C------------------------------------------------------------------C
C
      Return
      End
```